Computational and experimental study of phase stability, cohesive properties, magnetism and electronic structure of TiMn2

ARTICLE *in* ACTA MATERIALIA · MARCH 2003

Impact Factor: 4.47 · DOI: 10.1016/S1359-6454(02)00497-4 · Source: OAI

Available online at www.sciencedirect.com
SCIENCE DIRECT®
Pergamon
Acta Materialia 51 (2003) 1239–1247
Acta MATERIALIA
www.actamat-journals.com

Computational and experimental study of phase stability, cohesive properties, magnetism and electronic structure of $TiMn_2$

X.Q. Chen [a], V.T. Witusiewicz [b], R. Podloucky [a,*], P. Rogl [a,**], F. Sommer [c]

[a] *Institut für Physikalische Chemie, Universität Wien, Währingerstr. 42, A-1090, Wien, Austria*
[b] *ACCESS e. V. RWTH Aachen, Intzestr 5, D-52072 Aachen, Germany*
[c] *Max-Planck-Institut für Metallforschung, Heisenbergstrasse 3, 70596, Stuttgart, Germany*

Received 3 July 2002; accepted 18 October 2002

Abstract

By an ab initio approach we calculated phase stability, cohesive and magnetic properties, and the electronic structure of $TiMn_2$ for the C14 and C15 Laves structure types. The nonmagnetic C14 phase is the ground state in accordance to experiment, whereas a metastable ferromagnetic C15 phase is predicted with a local magnetic moment of 0.78 μ_β for Mn. The energy of formation was measured by a calorimetric drop experiment resulting in a value of -86.76 ± 6.79 kJ mol^{-1} at 298 K being in good agreement to the ab initio result of -88.8 kJ mol^{-1}. Model calculations based on Miedema's approach failed to yield reasonable results. The calculated densities of states reveal strong hybridisation between Ti-like and Mn d-like states.

Keywords: Laves phases; Magnetic structure; Ab initio electron theory; Heat of formation for TiMn2; Electronic properties

1. Introduction

Ductilisation of Ti-Al duplex alloys by alloying with Mn has been the subject of numerous studies devoted to the development and optimisation of high strength intermetallics not only for aerospace applications but also for earth-bound turbine assemblies [1–4]. To provide a thorough basis for the investigation and thermodynamic calculation of the phase relations within the Ti-Mn-Al ternary, detailed knowledge of the binary boundary systems particularly of the Ti-Mn system is a prerequisite. A recent reinvestigation [5] of the Ti-Mn binary within the scope of phase relations of the Ti-Mn-N system showed serious discrepancies to the hitherto accepted data [6] of the Ti-Mn system, concerning the homogeneous regions and phase equilibria around the phases (α,β)TiMn as well as concerning the eutectoid decomposition temperatures of TiMn, $TiMn_3$ and $TiMn_4$. Also as a hydrogen storage material [7–9] the performance of Mn-

* Corresponding author. Tel.: +43-1-4277-52570; fax: +43-1-4277-52579.
** Corresponding author. Tel.: +43-1-4277-52456; fax: +43-1-4277-52456.
E-mail addresses: raimund.podloucky@univie.ac.at (R. Podloucky); peter.franz.rogl@univie.ac.at (P. Rogl).

1359-6454/03/$30.00 © 2003 Acta Materialia Inc. Published by Elsevier Science Ltd. All rights reserved.
doi:10.1016/S1359-6454(02)00497-4

Ti alloys is excellent, raising a particular interest in the exact phase equilibria of the Ti-Mn binary system. A thermodynamic modelling of the revised binary diagram Ti-Mn [5] suffered from the fact, that the thermodynamic heat of formation for $TiMn_2$ was so far not well established in the literature. The thermodynamic calculation of the phase equilibria in the ternary system Ti-Mn-N based on thermodynamic modelling of the binary systems Mn-N and Ti-N, required a heat of formation of $TiMn_2$ significantly more negative than that obtained from the estimation based on Miedema's model [10]. A reliable thermodynamic basis for a high-quality thermodynamic optimization of the systems Ti-Mn, Ti-Mn-N and Ti-Mn-Al can thus only be obtained from a sound thermodynamic measurement such as drop calorimetry in combination with a density functional calculation of the heat of formation of $TiMn_2$.

Recently, a series of Laves phase AB_2 metal hydride electrodes based on C15-type Ti(Zr)-Ni, $Zr(Mn,Ni)_2$ were studied [11–13]. It is furthermore interesting to note, that partial substitution of Zr by Ti, V and Co in $ZrMn_2$ stabilized the C15-type structure [14], thereby triggering interest in the metastable C15-type Laves phase for $TiMn_2$. Literature data concerning the metastable C15 phases of $TiMn_2$, however, are very scarce.

Few theoretical studies have hitherto been undertaken for group IV Laves phases of C14 structure. Ishida et al. [15] calculated the density of states of $TiMn_2$ from which the authors derived that $TiMn_2$ is paramagnetic. Applying a tight-binding approach, Yamada [16] reviewed magnetic properties of the transition metal Laves compounds with the cubic C15 structure but no data are given for $TiMn_2$ [16]. Early magnetisation and susceptibility measurements for $TiMn_2$ yielded a large effective magnetic moment for Mn of 2.7 μ_β [17], in conflict with the theoretical results of Ishida et al. [15]. Experimental data suggest that the C14 Laves phase $Ti_{1.2}Mn_{1.8}D_3$ forms ferromagnetic layers [18].

No attempts have been made so far to apply a state-of-the-art ab initio approach for a comprehensive study of energetical, structural and magnetic properties of $TiMn_2$.

2. Computational details

The calculations were done in the framework of density-functional theory (DFT) using the generalized gradient approximation (GGA) of Perdew and Wang [19] including the approach of Vosko, Wilk and Nusair [20] for magnetic systems. The present results were obtained using the VASP code with projector augmented wave potentials (PAW) [21]. Brillouin-zone integrations were performed on a suitable grid of Monkhorst–Pack special points [22]. Optimization of geometrical parameters (atomic positions and lattice parameters) was achieved by minimizing forces and total energies. The c/a ratio for the hexagonal C14 phase was optimized by a stress tensor technique. The data of standard DFT calculations like ours refer to 0K if taken rigorously and should be compared to experimental data for sufficiently low temperatures. Magnetic properties were investigated by allowing for spontaneous spin polarization.

Calculations of local atomic-like quantities such as local density of states and local magnetic moments were made inside spheres centered at the atomic sites. Their radius was chosen to be the Wigner–Seitz radius corresponding to a given volume. Due to the spherical symmetry inside these spheres quantities can be expanded into spherical harmonics and therefore 1-like characters can be attributed.

For the class of compounds including $TiMn_2$ two structure types compete. Its ground state structure is the hexagonal Laves C14 type ($MgZn_2$-type, space group $P6_3/mmc$). The unit cell contains 8 Mn atoms in two crystallographically independent sites (2a) and (6h). Furthermore, we also considered the Laves C15 type ($MgCu_2$-type, space group $Fd\bar{3}m$). Possible magnetic phases were studied by nonmagnetic (NM), ferromagnetic (FM) and selected antiferromagnetic (AF) spin arrangements in suitable supercells.

For the derivation of formation energies, the total or cohesive energies of the pure phases are needed. The low-temperature ground state α phase of solid Mn is, however, intractable for high-precision calculations because of its complex magnetic structure. However, a high-temperature metastable fcc γ Mn phase occurs at temperatures of

≈1400K. One therefore expects that the cohesive energies of the α and γ phases are rather similar. At low temperatures when a tetragonal structure is stabilized by alloying or epitaxy, the γ phase becomes antiferromagnetic [23]. Accordingly, we made a spin polarized calculation for γ-Mn assuming a parallel and antiparallel spin arrangement in alternate sheets perpendicular to the c-axis [24,25].

3. Results and discussion

3.1. Cohesive properties

3.1.1. Ab initio cohesive and formation energies

The cohesive energy per formula unit of a binary compound A_MB_N is obtained by

$$E_{coh}^{A_MB_N} = E_{total}^{A_MB_N} - [ME_{atom}^{A} + NE_{atom}^{B}], \quad (1)$$

where $E_{total}^{A_MB_N}$ refers to the total energy of the intermetallic compound at equilibrium, and E_{atom}^{A}, E_{atom}^{B} are the total energies of the pure atomic constituents. At zero temperature, because there is no entropy contribution, the free energy of formation is derived by the energy difference

$$\Delta H^{A_MB_N} = E_{total}^{A_MB_N} - [ME_{solid}^{A} + NE_{solid}^{B}]. \quad (2)$$

The quantities E_{solid}^{A} and E_{solid}^{B} are the total energy of the solid elemental constituents. Table 1 summarizes the ab initio formation enthalpies and cohesive energies including the experimentally derived values as well as the results predicted by Miedema's model [10]. The comparison for C14 $TiMn_2$ shows that the experimental result for the heat of formation is in good agreement with the ab initio data. However, there is a large deviation of Miedema's value. Concerning ab initio cohesive energies the DFT data are too negative (≈10% for Ti, ≈30% for Mn in comparison to Ref. [26]) due to the well-known shortcomings of the approximations to DFT. Therefore, for the ab initio cohesive energy of $TiMn_2$ one expects an error of comparable size. In general, total energies of free atoms carry the largest errors whereas the solid phases are much better described. Therefore, DFT energies of formation are much more reliable.

3.1.2. Calorimetric data and related results

The measurements were performed using a laboratory built high temperature isoperibolic calorimeter [27]. The heat of dissolution $\Delta H_{diss,i}$ of pure Mn, Al and $TiMn_2$ was measured by dropping of solid samples at room temperature (i.e. 298 K) into liquid Al at a temperature of 1409±3 K. The induced total heat effect per mole is

$$\Delta H_{diss,i} = \Delta H_{298,i}^{1409} + \Delta H_{fus,i} + \Delta \bar{H}_i, \quad (3)$$

where $\Delta \bar{H}_i$ is the partial enthalpy of mixing of component i (i = Mn, $TiMn_2$, Al) in the Ti-Al-Mn, Al-Mn systems. The quantity $\Delta H_{fus,i}$ denotes the molar heat of fusion of component i, and $\Delta H_{298,i}^{1409}$ the enthalpy change of component i upon heating from 298 K to the measurement temperature 1409 K.

The dissolution experiment was started by dropping several samples of pure solid Al at room temperature into liquid Al. In order to determine the

Table 1
Calculated heats of formation ΔH, cohesive energies E_{coh} per formula unit for Ti, Mn, $TiMn_2$, and experimental data. Result for C15 phase refers to the ferromagnetic calculation

	Structure	ΔH (kJ mol^{-1})			E_{coh} (eV)
		Ab initio	experiment	Miedema	ab initio
Ti	A3	0	0	0	−5.28
TiMn2	C14	−88.8	−86.76±6.79[a]	−26.56	−13.92
TiMn2	C15	−85.9	—	—	−13.87
Γ-Mn	A_a	0	0	0	−3.86

[a] Experimental data of present work at 298 K.

composition dependent calibration factor W [28], A1 samples were dropped further after each dropping of Mn and $TiMn_2$ samples, respectively. Then $\Delta H_{diss,i}$ values for Mn, $TiMn_2$ and Al samples were calculated from the area F_i under a temperature-time curve using the relation [28]

$$\Delta H_{diss,i}(y) = W(y)F_i(y) \tag{4}$$

in which y is the molar fraction of Mn or $TiMn_2$ in the dilute liquid Al-Mn or AlMn-Ti alloys, respectively. For the numerical solution of the differential equation,

$$dW(y) = -\frac{W(y)}{f(y)}(df(y) + [F_i(y) - F_{Al}(y)]dy), \tag{5}$$

the boundary condition (realising that the initial liquid is pure Al) is then

$$W(y = 0) = \Delta H^{1409}_{298,Al}/F_{Al}(y = 0), \tag{6}$$

defining $f(y) = yF_i(y) + (1-y)F_{Al}(y)$. The value of $\Delta H^{1409}_{298,Al}$ was adopted from the SGTE database [29]. For the evaluation of the integral enthalpy of formation ΔH of liquid Al-Mn and Al-Mn-Ti alloys due to dropping of solid samples from 298 K into liquid, the equation

$$\Delta H(y) = \frac{\Sigma_k(\Delta H^k_{diss,i}(y)\Delta n_k)}{n_0 + \Sigma_k \Delta n_k} \tag{7}$$

was applied. There, n_0 denotes the number of moles of pure Al, Δn_k the number of moles of sample k dropped into the liquid bath, and k the number of the sample in the series of one run, respectively. The obtained data of ΔH are shown in Figs. 1(a) and (b).

The integral values are fitted by

$$\Delta H = y(1-y)(A + By) + (1-y)C. \tag{8}$$

The coefficients A, B and C are determined by a least-squares analysis (Table 2, Fig. 1). The coefficient C corresponds to $\Delta H^{1409}_{298,Al}$ according to Ref. [29], whereas A denotes the enthalpy of dissolution of component i at infinite dilution, namely $\Delta H^{\ominus}_{diss,i}$.

The enthalpy content of undercooled liquid Ti at 1409 K ($\Delta H^{1409}_{298,Ti} + \Delta H_{fus,Ti}$) was evaluated using the SGTE database for pure elements [29], which resulted in 47.127 kJ mol^{-1}. The enthalpy of dissolution of pure Ti at infinite dilution was evaluated according to Eq. (3) using the direct calorimetric measurements of Ref. [30] as well as the thermodynamically optimized Al-Ti database of Ref. [31] resulting in $\Delta H^{\ominus}_{diss,Ti} = -88.874$ and -91.064 kJ mol^{-1}, respectively. The value of -88.874 kJ mol^{-1} was then taken for the following derivation.

Table 2
Values of fitting parameter A in Eq. (8)

Sample	A (kJ mol^{-1})	Error A (2σ) (kJ mol^{-1})	Ref.
Mn	−6.843	0.078	present work
$TiMn_2$	−15.798	2.228	present work
Ti	−88.874	6.408	evaluation[a]
Ti	−91.064	—	evaluation[b]

[a] Derived from calorimetric measurements [30].
[b] Derived from calculated thermodynamically optimized Ti-Al database [31].

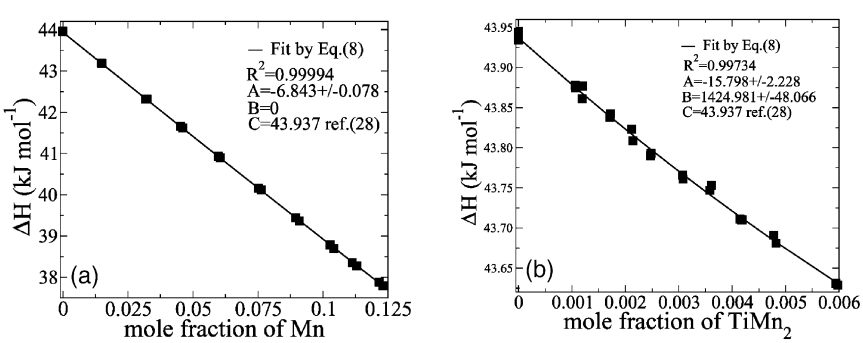

Fig. 1. Measured integral enthalpy of formation of liquid Mn-Al (panel a) and Ti-Mn-Al alloys (panel b) due to dropping of solid samples of Al and Mn (panel a), Al and $TiMn_2$ (panel b) at 298 K into liquid Al at 1409±3 K, respectively.

The enthalpy of formation of compound $TiMn_2$ at 298 K was evaluated using the values of $\Delta H^{\ominus}_{diss,i}$ according to

$$\Delta H^{\ominus}_{298} = 2\Delta H^{\ominus}_{diss,Mn} + \Delta H^{\ominus}_{diss,Ti} - \Delta H^{\ominus}_{diss,TiMn_2} \quad (9)$$

which finally results in $\Delta H^{\ominus}_{298} = -86.762$ kJ mol^{-1} with a standard error of $2\sigma = \sqrt{0.078^2 + 2.228^2 + 6.408^2} = 6.785$ kJ mol^{-1} as listed in Tables 1 and 2.

Figure 2 compares the heat of formation calculated on basis of Miedema's model with calorimetric data at 2000 K[30] for a liquid Ti-Mn binary alloy. Obviously, the fitting values using the present experimental data are in agreement with early calorimetric data, while Miedema's model is unsatisfactory.

3.2. Structural properties and electronic structure

For both structure types, C14 and C15, volume dependent total energies for several magnetic states (NM, FM, AM) were calculated (Fig. 3). Table 3 summarizes the calculated results for the equilibrium state and compares to experimental data where available. Our theoretical results agree reasonably well with available experimental values. The calculated volume of the C14 equilibrium phase is smaller by about 4% than the experimental value which is attributed to the shortcomings of the approximations of the exchange-correlation functional of DFT in spite of the GGA approach which in many cases is improving the overbinding effects of the local density approximation. However, because of the localized nature of the Mn d-like states the improvements are not fully sufficient concerning the volume.

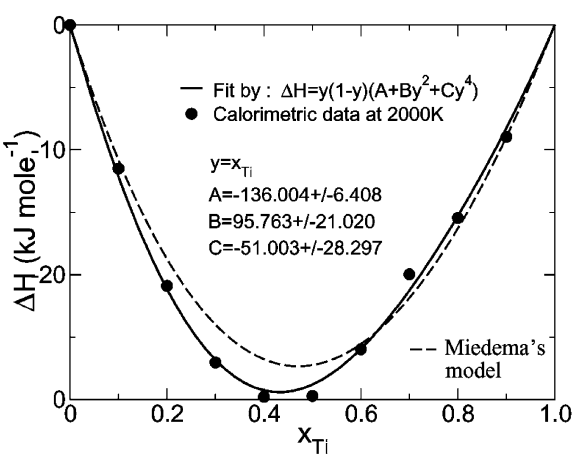

Fig. 2. Integral enthalpy of mixing of liquid Mn-Ti alloys. Comparison of calorimetric data with calculated data based on Miedema's model.

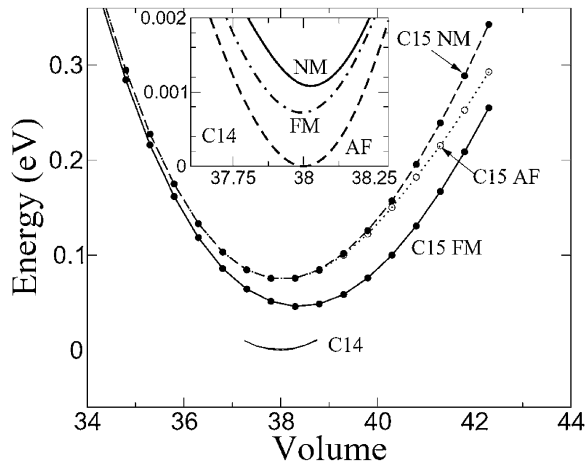

Fig. 3. Ab initio total energy per formula unit versus volume in Å^3 per formula unit for several magnetic phases (see text) of $TiMn_2$ with C14 and C15 structure types. Zero of energy: energy minimum for C14. Insert: results for C14 on enlarged scale.

For C15 $TiMn_2$ the equilibrium volumes of the FM and NM phases are 12.77 and 12.60 Å^3 per atom, respectively. The larger volume of the magnetic phase is due to the magnetovolume effect of electronic states with parallel oriented spins which generates a magnetic pressure due to Pauli's principle.

There is a close structural relation between both Laves phases [34]. Seven out of eight atomic layers are identical for both structures ([111] stacking of C15 compared to [0001] stacking of C14) [35]. As a consequence the hexagonal lattice constant $a(C14)$ is smaller by a factor $1/\sqrt{2}$ than $a(C15)$. From this relation, a value of $a(C14) = 4.76$ Å is obtained from the cubic lattice parameter which is close to the ab initio result in Table 3.

Averaged bond lengths of the hexagonal C14 structure are derived from nearest-neighbour distances for Mn-Mn, Mn-Ti, and Ti-Ti bonds,

Table 3
Ab initio calculated bulk properties (lattice parameters, bulk moduli B_0) of Ti, Mn, and $TiMn_2$ in comparison to available experimental values

	Structure	[a (Å)]		[c/a]		[B_0 (Mbar)]	
		calc.	exp.	calc.	exp.	calc.	exp.
Ti	A3	2.94	2.95[a]	1.586	1.586[a]	1.16	1.l[b]
$TiMn_2$	C14	4.69	4.82[c]	1.668	1.642[c]	2.07	
$TiMn_2$	C15	6.74				2.03	
Mn	A_a	3.62	3.79[d]	0.956	0.946[d]	0.85	0.60[b]

For C15 $TiMn_2$ the values refer to the ferromagnetic calculation; for A_a Mn the antiferromagnetic spin arrangement was chosen (see text).
[a] Ref. [32].
[b] Ref. [26].
[c] Ref. [18].
[d] Ref. [33].

respectively, which are in very good agreement to the values for C15 in Table 4.

Considering the energy of formation (Table 1) the agreement between the measured and the ab initio value is good. The comparison of the bulk modulus B_0 for pure γ Mn has to be made with care because the experimental value of 0.60 Mbar concerns the ground-state α phase of Mn. However, Table 3 indicates that the calculated value of 0.85 Mbar is presumably too large. We would expect that the bulk modulus B_0 of the C14 structure is also overestimated but there is no experimental value available in literature. For pure Ti, the agreement between the ab initio data and measured values is — as expected — excellent because the 3d-states of Ti are much less localized than for Mn, and a local approximation to the many-body terms of DFT such as GGA is much more reliable.

As shown by Fig. 3 for the C14 structure at the equilibrium volume the total energy curves for nonmagnetic and magnetic cases nearly coincide. However, according to Stoner's criterion of band magnetism ($I{\cdot}n(E_F) > 1$ with $I{\approx}1$ eV) C14 $TiMn_2$ is close to spin polarization as is expressed by the large value of the density of states (DOS) of the NM case at Fermi energy (upper half of Fig. 4(a) and Fig. 5(a)).

Table 4
Bonds, local coordination and calculated nearest-neighbour bond lengths for nonmagnetic and ferromagnetic C15 $TiMn_2$

Bond	Coordination	Bond Lengths (Å)		
	C15	C15 FM	C15 NM	C14 NM
Mn-Mn	6	2.38	2.37	2.40
Mn-Ti	6	2.79	2.78	2.78
Ti - Ti	4	2.92	2.91	2.91

Last column: averaged bond lengths for the C14 structure.

Table 6 reveals that the value of $n(E_F)$ for Mn(2a)-like states is close to the critical Stoner limit in contrast to Mn(6h)-like states which is caused by the different local environments of these two sites. Site Mn(2a) has only 3 Ti nearest-neighbours (with distance 2.76 Å) available for hybridisation whereas Mn (6h) has in total nine Ti neighbours (with distances of 2.76 Å six-fold coordinated and 2.83 Å three-fold coordinated). Furthermore, the Mn(2a)-Mn bond length is 2.44 Å (six-fold coordinated) whereas Mn (6h)-Mn bonds are partially shorter, namely 2.44 Å, 2.42 Å and 2.27 Å, each one two-fold coordinated. (For the sake of completeness, the Ti-Ti bond lengths are 2.89 Å three-fold coordinated and 2.97 Å (one-fold coordinated). All these ab initio distances agree within 2% to the experimental values of Ref. [18]) The different local environments of the Mn sites are also visualized by the local DOS in Fig. 5(a). In particular, close to Fermi energy the Mn (6h)-like DOS is split into two peaks which merge for the Mn (2a)-like DOS resulting in a significantly larger value of $n(E_F)$ for Mn(2a). Also Mn-

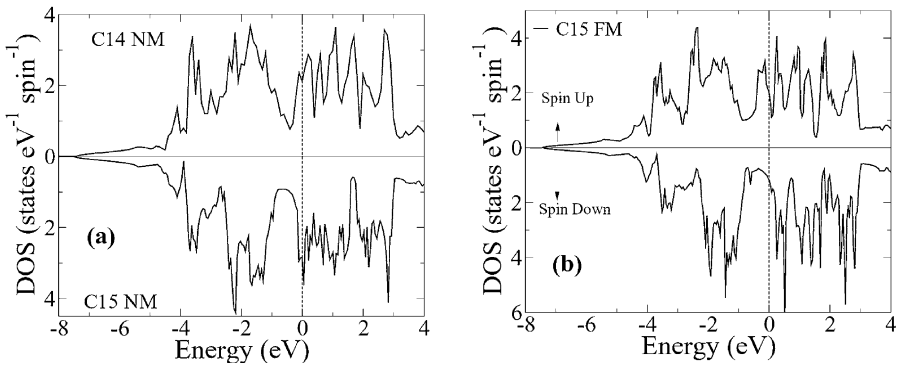

Fig. 4. Ab initio total DOS of C14, C15 nonmagnetic and C15 ferromagnetic phases of $TiMn^2$ per formula unit. Energy scale relative to Fermi energy.

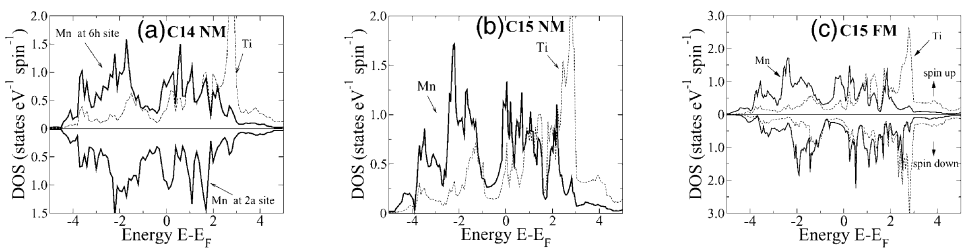

Fig. 5. Site projected d-like local DOS for nonmagnetic C14 and C15 structures of $TiMn_2$, panels (a) and (b), respectively; Upper half of panel (a): local DOS for site Mn (6h); lower half of panel (a): local DOS for site Mn(2a). Local d-like DOS for ferromagnetic C15 in panel (c) split into spin-up and down states. Energy scale relative to Fermi energy.

Table 5
Ab initio 1-like local magnetic moments in μ_B for the ferromagnetic phase of C15 $TiMn_2$

Atom	s	p	d
Mn	0.01	−0.02	0.79
Ti	−0.01	−0.03	−0.16

Ti hybridisation features are different, e.g. at about −1 eV. The AF spin structure is slightly favoured by less than 1 meV (insert of Fig. 3) with maximum local moments of Mn in the order of 0.05 μ_B.

In the metastable C15 structure $TiMn_2$ is becoming ferromagnetic because of the large value of $n(E_F)$ (lower half of Figure 4(a) and Figure 5(b)). Table 6 for the C15 NM case gives a value for Mn-like $n(E_F)$ which is about 10% larger than for Mn(2a) in the C14 structure. Obviously (because the selfconsistent ab initio calculation resulted in a net magnetic moment of about 0.8 μ_B), this value is above the critical Stoner limit. Figures 4(b) and 5(c) shows the spin projected DOS for FM C15 split into majority (or up spin) and minority (or down spin) states. The spin splitting is due to the exchange splitting of Mn d-like states which amounts to 0.68 eV as calculated by the difference of the average occupied band energy of Mn d-like spin-down and spin-up bands. The states responsible for the magnetism are clearly visualized by the peak of occupied states about −0.5 eV as shown by the spin polarized DOS. The integration of this peak gives about 0.8 spin-up electrons. The induced magnetic moment for Ti of opposite orientation (Table 5) mainly comes from a peak of the Ti-like DOS at −1.5 eV (lower half of Fig. 5(c)).

The energy difference of the C15 FM phase to the stable C14 phase is ≈0.05 eV per formula unit corresponding to ≈500 K. The magnetic energy

Table 6
Ab initio 1-like local and total DOS at Fermi level for the nonmagnetic C14, C15 and ferromagnetic C15 phases

Phase	atom	s	p	d	Total
C14 NM	Mn(2a)	0.01	0.05	0.95	
	Mn(6h)	0.01	0.04	0.75	
	Ti	0.01	0.02	0.12	
					2.16
C15 NM	Mn	0.01	0.05	1.10	
	Ti	0.01	0.02	0.48	
					2.94
C15 FM spin-up	Mn	0.0	0.03	0.82	
	Ti	0	0.01	0.21	
					2.0
C15 FM spin-down	Mn	0.0	0.04	0.39	
	Ti	0	0.02	0.23	
					1.18

Local DOS in states eV^{-1} $spin^{-1}$ per atom; total DOS in states eV^{-1} $spin^{-1}$ per formula unit.

gain is 0.03 eV per formula unit according to the difference between C15 NM and FM energy minimum. According to Table 3 due to the magnetic pressure the atomic volume of the C15 structure is larger by 1% than for C14 but the bulk modulus is smaller by 2% reflecting the weaker bonding of the magnetic metastable structure.

Figures 4 and 5 show distinct features of the total and d-like DOS. In all cases a pronounced minimum about 1 eV below Fermi energy occurs separating the energy regions of bonding and antibonding states. Below Fermi energy Mn d-like states dominate due to the lower lying atomic level as compared to Ti assuming no sizeable charge transfer from Ti to Mn. The filling of the Mn d-like states amounts to $\approx$5.5 electrons. Strong hybridization of Mn and Ti d-like states is clearly demonstrated by the DOS for energies from -5 eV to 2 eV exhibiting features similar for both types of atoms. A very large peak of unoccupied Ti d-like states arises at 3 eV which is due to nonbonding states.

Discussing the NM DOS (Fig. 4) the structural competition in favour of C14 compared to C15 is supported by the values of $n(E_F)$ being significantly smaller for C14 namely 2.16 states eV^{-1} per spin and formula unit compared to a value of 2.94 for C15 (Table 6). As mentioned above, for C15 the large value of $n(E_F)$ leads to spin polarization; the magnetic energy gain, however, is too small to stabilize the C15 structure.

4. Conclusion

In the present paper, results of a detailed study on structural and phase stabilities, cohesive and magnetic properties as well as bonding properties for the two structure types C14 and C15 of $TiMn_2$ are presented. The stability of the C14 structure is quantified by state-of-the-art ab initio calculations revealing that a possibly high temperature metastable C15 phase would be ferromagnetic. The calculated lattice parameters and heat of formation are found to be in good or reasonable agreement with available experimental results for $TiMn_2$. Furthermore, experimental results of a calorimetric determination of the heat of formation of $TiMn_2$ is also presented together with applications of Miedema's model which turns out to be not reliable for $TiMn_2$. The electronic structure is discussed in terms of the density of states revealing strong hybridisation of Ti and Mn d-like states. The large value of the density of states at Fermi energy for the C15 compound leads to spin polarization with local Mn moments of 0.78 μ_B and sizeable antiparallel moments of -0.20 μ_B for the Ti atoms. On the other hand, the C14 phase is on the brink to become magnetic.

Acknowledgements

Work supported by the Austrian Science Fund (FWF) project No.P14761. The authors also thank the Chinese-Austrian Scientific Technical exchange program V A.15 for a research grant (X.Q. Chen). The support of the Center of Computational Materials Science (CMS) in Vienna is gratefully acknowledged. Part of the calculations were performed on the Schrödinger I PC cluster of the University of Vienna. We thank M. Marsman, G. Kresse and G. Schneider for many fruitful discussions.

References

[1] Huang ZW, Bowen PC. Scripta Mater 2001;45:931; Rudolf T, Skrotzki B, Eggeler G, Bowen P. J. Mater. Sci. Eng. A 2001;815:A319–321; Liu CM, Xia K, Li W. J. Mater. Sci. 2000;35:975; Jan W, Wu GY, Wei H-S. Phys. Rev. B 2001;64:165101; Yanga M-R, Wu SK. Acta Mater 2002;50:691.
[2] Sikora T, Hug G, Jaouen M, Rehr JJ. Phys. Rev. B 2000;62:1723.
[3] He Y, Schwarz RB, Migliori A. J. Mater. Res 1995;10:1187.
[4] Taub AI, Fleischer RL. Science 1989;243:616; Liu CT, Stiegler JO. Science 1984;226:636.
[5] Bittermann H, Rogl P, Krendelsberger R, Ding X, Weill F, Chevalier B, Etourneau J, Saccone A, Ferro R. J. Phase Equilibria (to be published).
[6] Saunders N. System Mn-Ti. In: Ansara I, Dinsdale T, Rand MH editors. COST 507, Concerted Action on Materials Sciences, Thermochemical Database for Light Metal Alloys. EUR 18499EN, European Commission, Directorate-Genera 1 XII Science, Research and Development, Luxembourg 1998;2:241.
[7] Ivey DG, Northwood DO. Z. Phys Chem. Bd 1986;147:191.
[8] Matsumura T, Yukawa H, Morinaga M. J. Alloys Comp 1998;279:192.
[9] Hempelmann R, Hilscher G. J. Less Comm. Metal 1980;74:103.
[10] Miedema AR. Physics B 1980;100:201; de Boer FR, Boom R, Mattens WCM, Miedema AR, Niessen AK. Cohesion in metals, transition metal alloys. Amsterdam: Elsevier, 1989; Niessen AK, de Boer R, Boom R, de Chatel RE, Mattens WCM, Miedema AR. CALPHAD 1983;7:51.
[11] Moriwaki Y, Gamo T, Seri H, Iwaki T. J. Less-Comm. Met 1991;1211:172–4.
[12] Dong MK, Sang ML, Jae JH, Jang KJ, Lee JY. J. Electrochem. Soe 1998;145:93.
[13] Hsu YS, Chiou SL, Perng TP. J. Alloys Compounds 2000;313:263.
[14] Gröbner J, Pisch A, Schmid-Fetzer R. J. Alloys Comp 2001;433:317–8.
[15] Ishida S, Asano S, Ishida J. J. Phys. Soc. Jpn 1985;54:3925.
[16] Yamada H. Physica B 1988;149:390.
[17] Shavishvili TM, Meskhishvili AI, Andriadze TD. Phys. Met. Metall 1979;47:184.
[18] Hempelmann R, Wicke E, Hilscher F, Wiesinger G. Ber. Bunsenges. Phys. Chem 1983;87:48; Fruchart D, Soubeyroux JL, Hempelmann R. J. Less-Comm. Met 1984;99:307.
[19] Perdew JP, Wang Y. Phys. Rev. B 1992;45:13244.
[20] Vosko SH, Wilk L, Nusair M. Can. J. Phys 1980;58:1200.
[21] Kresse G, Furthmüller J. Comput. Mater Sci. 1996;6:15; Phys. Rev. B 1996;54:11169; Kresse G, Joubert D. Phys. Rev B 1999;59:1758.
[22] Monkhorst HJ, Pack JD. Phys. Rev. B 1976;13:5188.
[23] Qiu SL, Marcus PM, Ma H. Phys. Rev. B 2000;62:3292.
[24] Asada T, Terakura K. Phys. Rev. B 1993;47:15992.
[25] Meneghetti D, Sidhu SS. Phys. Rev 1957;105:130.
[26] Kittel C. Introduction to Solid State Physics, 5th edition, New York: Wiley, 1976).
[27] Sommer F, Schott J, Predel B. Z Metallkd 1985;76:369.
[28] Witusiewicz VT, Ivanov MI. J. Alloys Comp 1993;200:177.
[29] Dinsdale AT. CALPHAD 1991;15:317.
[30] Esin YuO, Bobrov NP, Petrushevski MS, Geld PV. Izv AN SSSR. Metally 1974;5:104.
[31] Ohnuma I, Fujita Y, Mitsui H, Ishikawa K, Kainuma R, and Ishida K. Acta Mater, 2000:48,3113.
[32] Young DA. Phase diagrams of the elements. Berkeley: University of California, 1991.
[33] Endoh Y, Ishikawa Y. J. Phys. Soc. Jpn 1971;30:1614; Wyckoff RWG. Crystal structure. New York: Wiley, 1963; Wijn HPJ, editor. Landdolt-Bömstein, New Series, Group III. Magnetic properties of metals, 19. Berlin: Springer; 1971. p. 1-7.
[34] Komura Y. Acta Crystallogr 1962;15:770.
[35] Irodova AX, Suard E. J. Alloys Comp 2000;299:32.